SAND84 — 1957
Unlimited Release
Printed May 1985

Distribution
Category UC — 92

Preliminary SPR Thermal Model Description and Results for WH-11 and BM-4

David Tomasko
Strategic Petroleum Reserve Geotechnical Division
Sandia National Laboratories
Albuquerque, NM 87185

Abstract

Fluid temperatures within the Strategic Petroleum Reserve caverns are calculated using a modified one-dimensional, time-dependent Rahm-Walin equation coupled to a two-dimensional, time-dependent heat conduction equation in the salt massif. Comparisons of model results with experimental data from West Hackberry Cavern 11 and Bryan Mound Cavern 4 are very good for up to eight years of cavern life.

Preliminary SPR Thermal Model Description and Results for WH-1 1 and BM-4

Background

We are developing a thermal model for predicting the fluid temperature distributions within the Strategic Petroleum Reserve (SPR) caverns. Information from this model will be useful for salt creep modeling, cavern pressure interpretation, and for developing appropriate monitoring procedures.

Contents of Report

In the remainder of this report, we will describe a preliminary thermal model for the SPR caverns and compare model calculations with experimental data from West Hackberry Cavern 11 (WH-11) and Bryan Mound Cavern 4 (BM-4).

Contents

Contents

The material presented in this report is arranged in the following order:

Figures

Tables

Executive Summary

Format of Summary

The summary of this report consists of two sections:

- Description of model
- Comparison of model with data

These sections are given below.

Summary of Model Description

The Sandia National Laboratories SPR thermal model uses the following solution methods and features:

- A fully implicit, two-dimensional, axially symmetric time-dependent solution in the salt
- A fully implicit, two-dimensional, axially symmetric time-dependent solution in the anhydrite/brine porous media layer that underlies the caverns
- A fully implicit, one-dimensional, time-dependent Rahm-Walin solution in the oil/brine fluids of the caverns
- A heat exchanger model to calculate the increase in oil temperature during cavern fill
- A fluid-mixing model to calculate fluid mixing caused by Rayleigh-Taylor instabilities
- An energy-correction model that ensures conservation of energy

Comparison of Data

Comparisons of our thermal model results with experimental data from WH-11 and BM-4 are very good, especially within the axial isothermal zones evident in both caverns (temperatures predicted by our model are within $\sim 2\ \%$ of the isothermal temperature measured). Uncertainties in the temperature measurements and approximations used in the model can easily explain the observed temperature differences.'

The worst agreement between the model predictions and the experimental data occurs at the top of the cavern. This disagreement is expected because of the following factors:

- Our mixing model is sensitive to the axial cell size used (constant mesh size is now required).
- The thermal measurements are usually worst near the top of the cavern.
- Measurements above the roof of the cavern do not represent salt conditions calculated by the model.

For both comparisons presented, the time-dependent thermal rise is well predicted and other physical processes appear to be well simulated.

Nomenclature

English

A	Cavern cross-sectional area (ft^2)
C_p	Specific heat (Btu/lb °F)
d	Rahm-Walin wall thickness (ft)
g	Gravitational constant (32.17 ft/s^2)
K	Thermal conductivity (Btu/h °F ft)
L	Rayleigh number scaling length (ft)
M_0	Volumetric flux (ft^3/h)
r	Radial distance from centerline of cavern (ft)
S_o	Source coefficient in Rahm-Walin equation defining the wall boundary condition = $\frac{K_{salt}}{K_{oil}\, d} = \frac{K_{salt'}}{K_{oil}\, Ar \cos\theta}$ (ft)
t	Time (h)
T	Temperature (°F)
$\hat{T}$	Salt temperature at the salt/fluid boundary (°F)
z	Vertical distance measured from total depth (ft)

Greek

α	Thermal diffusivity = $K/C_p\rho$ (ft^2/h)
β	Volumetric thermal expansion coefficient (1/°F)
Δr	Finite difference approximation to the differential dr (ft)
AZ	Finite difference approximation to the differential dz (ft)
ν	Kinematic viscosity (ft^2/s)
ρ	Density (lb/ft^3)
θ	Wall angle with respect to vertical
ϕ	Porosity of anhydrite/brine layer

Subscripts

I	Radial mesh coordinate
J	Axial mesh coordinate
I_{MAX}	Radial mesh coordinate for last radial node (r = maximum radius used in calculation = R_{MAX})
J_{MAX}	Axial mesh coordinate for last axial node (Z = maximum height of calculation from cavern total depth)

Superscripts

N	Value at time step N
N+1	Value at time step N+ 1

Description of Thermal Model

Computational Regions

Three computational regions are used in the Sandia thermal model:

- An outer zone composed of pure salt (Region 1)
- An inner zone containing oil and saturated brine (Region 2)
- An inner zone directly below Region 2 composed of anhydrite and saturated brine (Region 3)

Model Diagrams

Figures 1 and 2 illustrate the computational regions used in our thermal model.

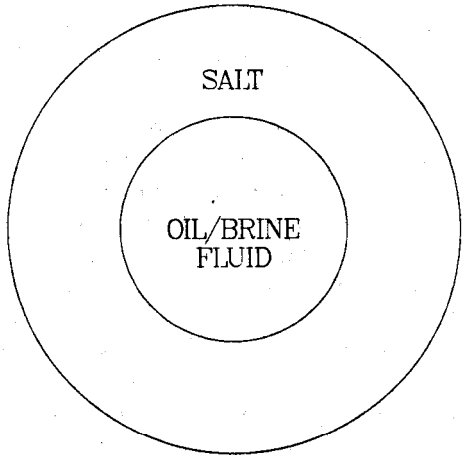

Figure 1. Model Plan View

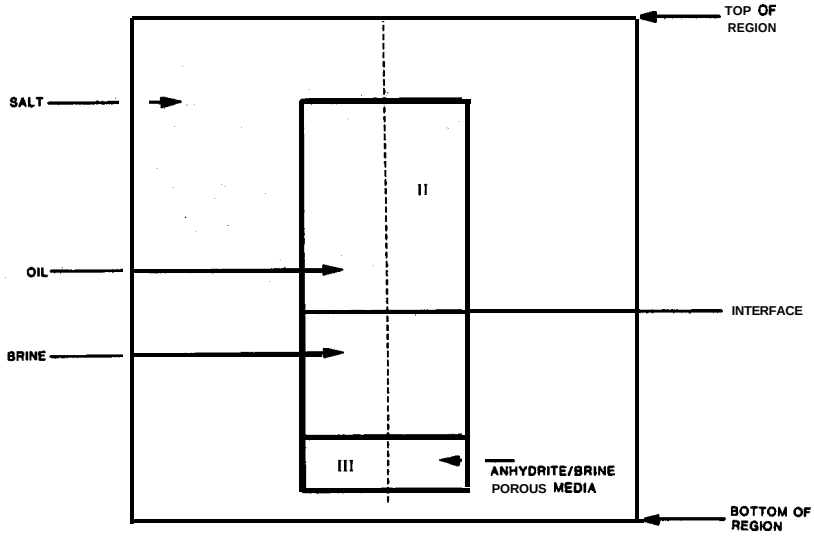

Figure 2. Side View of Model

Description of Thermal Model, Continued

Comments on Regions

Regions 1 and 2 and Regions 1 and 3 are concentric and axially symmetric. Region 3 lies directly below Region 2 and has a typical thickness of -200 ft.

The anhydrite in this layer is composed of unconsolidated particles which were not carried out of the cavern along with the saturated brine but settled to the bottom of the cavern during the leaching process. The anhydrite impurities present in the salt domes do not dissolve significantly during leaching because anhydrite is much less soluble than salt at the same temperature and pressure.[2]

Regional Details

The following details are important for understanding and defining the computational zones:

- Region l-The first region is treated as if it were entirely composed of salt (NaCl). The small quantities of impurities present [-5% anhydrite ($CaSO_4$)] are ignored.
- Region 2-The second zone contains two fluids: oil and brine. The brine is assumed to be saturated at its temperature and pressure. The two fluids are assumed to remain separate at all times, and an oil/brine interface of negligible thickness delineates the boundary between them.
- Region 3-The last region is a porous media composed of anhydrite crystals deposited during leaching and voids filled with saturated brine. The thickness of this layer varies from cavern to cavern, and can attain a thickness of 400 ft. Although this layer can be fairly thick, the anhydrite crystals will probably not lithify because of insufficient effective pressure, especially near the upper surface. The porosity (ϕ) of this layer has not been measured, but it should be similar to naturally deposited sand (porosity in the range of 25% to 50%).[3]

Assumption of Axial Symmetry

All three computational regions are treated using axial symmetry. We make this assumption for the following reasons:

- The salt is essentially homogeneous and isotropic (the volume fraction of insolubles, mostly anhydrite, is small (5% to 7 %), and the physical properties of the anhydrite are similar to those of salt).
- The anhydrite deposited during leaching should be nearly isotropic and homogeneous.
- There are no indications of any significant azimuthal temperature variations within the cavern fluids, based on the small amount of experimental data that we have on this subject.[1]

Description of Thermal Model, Continued

Regional Methods of Calculation

Heat transfer mechanisms differ from region to region. The following table specifies the dominant mode of heat transfer used in modeling each region:

Table 1. Modes of Heat Transfer for SPR Caverns

Region	Mechanism of Heat Transfer
1	Conduction
2	Free and Forced Convection
3	Conduction

Regional Coupling

The following list describes the regional coupling used in the Sandia thermal model:

- Regions 1 and 2 are coupled at the wall and at the top of the cavern.
- Regions 2 and 3 are coupled at the saturated brine/porous media interface.
- Regions 1 and 3' are coupled at the wall and at the bottom of the porous media zone. In some calculations, the porous media section extends to the bottom of the calculational region. For these cases, Regions 1 and 3 are coupled only at the wall of Region 3.

Regional Models

Three heat transfer models are used to solve the time-dependent thermal problem for the cavern:

- Salt model
- Porous media model
- Fluid model

Each of these models will now be discused in detail.

Salt Model

Governing Equation

The time-dependent heat conduction equation solved for the salt annulus is written

$$\frac{\partial T}{\text{at}} = \frac{K}{C_p \rho} \nabla^2 T \qquad (1)$$

where

$$\nabla^2 T = \frac{1}{r} \frac{\partial \left(r \frac{\partial T}{\partial r} \right)}{\partial r} + \frac{\partial^2 T}{\partial Z^2} .$$

Description of Thermal Model, Continued

Salt Model (cont'd)

Thermal Properties

Thermal properties within the salt are assumed to be isotropic (direction-independent) and independent of temperature and pressure. The thermal properties used in our calculations for salt, saturated brine, and oil are listed in Table 2.[4,5]

Table 2. Material Properties

	Salt	Saturated Brine	Oil
Density (lb/ft^3)	134.35	74.0	51.0
Thermal Conductivity (K = Btu/h °F ft)	3.236	0.332	0.076
Specific Heat (C, = Btu/lb °F)	0.212	0.785	0.45

Effect of Insolubles

The effect of embedded insolubles in the salt is assumed to be insignificant because of the small quantity of insolubles present (5% to 7 %) and the similarity in physical properties between salt and anhydrite (NaCl and $CaSO_4$).

Finite Difference Form for Eq (1)

Eq (1) is solved using a finite difference scheme that uses constant spacing in the R and Z direction (AR and AZ are independent). A fully implicit formulation is used to reduce the number of time steps required to predict 30 or more years of cavern thermal behavior.

Eq (1) in Finite Difference Form

A finite difference approximation to Eq (1) is

$$\frac{(T_{I,J}^{N+1} - T_{I,J}^{N})}{\Delta t} = \frac{K}{C_p\rho}\left(\frac{T_{I,J+1}^{N+1} + T_{I,J-1}^{N+1} - 2T_{I,J}^{N+1}}{\Delta Z^2}\right) + \frac{K}{C_p\rho}\left(\frac{T_{I+1,J}^{N+1} + T_{I-1,J}^{N+1} - 2T_{I,J}^{N+1}}{\Delta r^2}\right) + \frac{K}{C_p\rho}\frac{1}{r}\left(\frac{T_{I+1,J}^{N+1} - T_{I-1,J}^{N+1}}{2\Delta r}\right). \quad (2)$$

Description of Thermal Model, Continued

Salt Model (cont'd)

Boundary Conditions for Salt

The following boundary conditions are required to solve Eq (2):

- The temperature in the salt at the start of the calculation (initial conditions)
- The temperature or heat flux at $r = 0.0$ (at cavern centerline)
- The temperature or heat flux at $r = R_{max}$ (outer perimeter of the calculational region)
- The temperature or heat flux at the cavern wall, top and bottom
- The temperature or heat flux at the top and bottom of the calculational region.

Initial Salt Temperature

The temperature of the salt at the beginning of the calculation is set equal to the local value of the geothermal gradient. In general, the geothermal gradient is not precisely known. In our letter to E. E. Chapple' we recommended obtaining more and better geothermal data for SPR sites at West Hackberry, Bryan Mound, Sulphur Mines, and Bayou Choctaw.

A temperature profile measured in Bryan Mound Well 111-A shows a geothermal gradient that might be similar to those at the other sites (Figure 3). Note the presence of a thermal anomaly at a depth of 1000 ft. This nonlinear temperature zone is assumed to be caused by residual heat from sulphur mining operations in the region more than 40 years ago. Such large temperatures overlying a cavern may strongly influence the thermal model calculations. A more current thermal profile is shown in Figure 4 for Big Hill Well 106-A. No significant thermal anomalies are apparent.

Boundary Condition at $r = 0.0$

At $r = 0.0$, symmetry allows us to set $T_{1,J} = T_{2,J}$ (zero heat flux across the cavern centerline).

Boundary Condition at $r = R_{max}$

At the outer perimeter of the salt annulus we again use a Neumann (gradient) boundary condition and assume a zero heat flux across the perimeter ($T_{IMAX,J} = T_{IMAX-1,J}$). Use of a constant temperature boundary condition (Dirichlet) at this location would require an unnecessarily large computational space to ensure that the distance to the perimeter was sufficient for the temperature to be treated as a constant.

Boundary Condition at the Cavern Wall, Top and Bottom

We assumed the temperature of the cavern wall, top and bottom, to be equal to the local temperature of the fluid at time t, thus coupling the inner and outer regions of the calculation.

Description of Thermal Model, Continued

Salt Model (cont'd)

Boundary Condition at **Top** and Bottom of Calculational Region

We assumed the temperature at the bottom of the calculational region to be constant and equal to the local value of the geothermal gradient. At the top of the calculational region, a Neumann condition is again used (zero flux assumed: $T_{I,JMAX} = T_{I,JMAX-1}$).

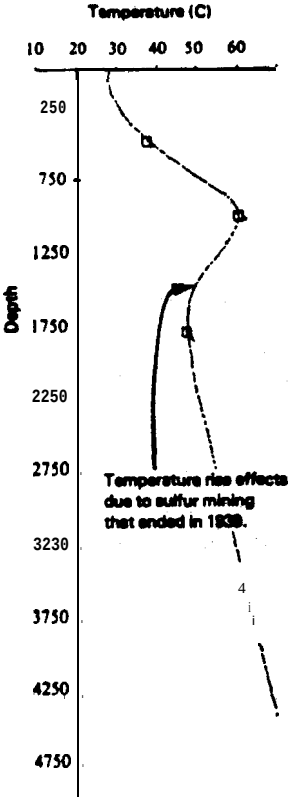

Temperature profile measured in brine well near Freeport, Texas. Digital record contains temperature values at 0.4-foot intervals, showing stable *resolution within less than ±0.01°C in constant temperature zone* (at *maximum temperature point). Thermal* anomaly at *1,000 feet is the stored residual heat from sulfur mining operations halted more than forty years* ago.

Figure 3. High-Resolution Temperature Profile for Bryan Mound Salt Dome Well 111-A

Description of Thermal Model, Continued

Salt Model
(cont'd)

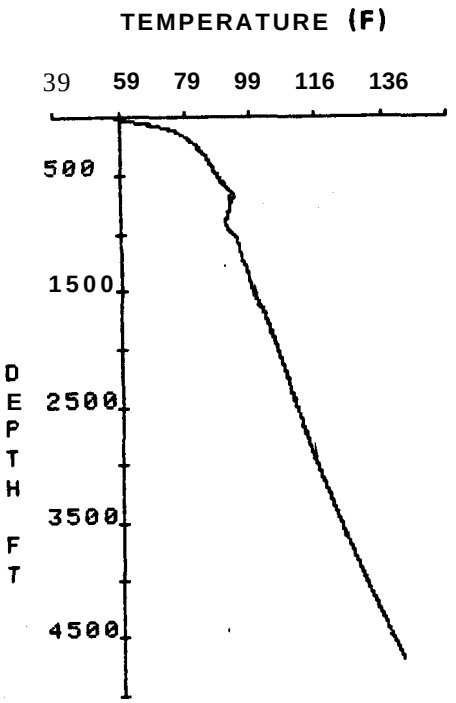

Figure 4. High-Resolution Temperature Profile for Big Hill Well 106-A

Description of Thermal Model, Continued

Porous Media Heat Transfer Model

The heat transfer model used within the porous media region is very similar to that used for the salt region, except that the thermal properties in the zone must reflect the effective value for anhydrite and saturated brine. Once effective values are calculated, they are used throughout the region.

Governing Equation

Heat conduction within the porous media is governed by the following equation:

$$\frac{\partial T}{\partial t} = \frac{K_{eff}}{C_{peff}\rho_{eff}} \nabla^2 T \tag{3}$$

where

$$\nabla^2 T = \frac{1}{r} \frac{\partial\left(r \frac{\partial T}{\partial r}\right)}{\partial r} + \frac{\partial^2 T}{\partial Z^2}$$

and subscript eff designates effective values.

Effective Thermal Properties

Effective values are required for the following thermal properties in order to solve the heat conduction equation in Region 3:

- Density (ρ)
- Specific heat capacity (C_p)
- Thermal conductivity (K)

Density

The effective density in a porous media having a porosity ϕ is given by[5]

$$P_{eff} = \rho_L \phi + (1 - \phi)\rho_s \tag{4}$$

where subscript L refers to the liquid phase and subscript s refer to the solid phase.

Specific Heat Capacity

The effective specific heat capacity at constant pressure for a porous media is given by[6]

$$C_{peff} = C_{pL}\phi + (1 - \phi) C_{ps}. \tag{5}$$

Thermal Conductivity

Effective thermal conductivity is given by the expression[6]

$$K_{eff} = K_L^{\phi} K_s^{(1-\phi)} \tag{6}$$

Description of Thermal Model, Continued

Porous Media Heat Transfer Model (cont'd)

Summary of Effective Values

Table 3 lists the effective thermal properties for a porous media as a function of porosity.

Table 3. Effective Values for Porous Media

ϕ (%)	K	C_p	ρ
0*	3.24	0.204	182.9
20	2.05	0.320	161.3
30	1.64	0.378	150.5
40	1.30	0.436	139.7
50	1.04	0.494	128.9
100†	0.33	0.783	74.9

*Solid anhydrite
†Saturated brine

Comments on Table

Compare the solid anhydrite thermal conductivity and specific heat capacity with those of salt (Table 2). They are practically the same. These similarities, coupled with a small volumetric fraction (5% to 7 %), allow us to disregard the impurities present in the salt region.

Method of Solution for Regions 1 and 3

Regions 1 and 3 are solved simultaneously because of the similarities between their respective governing equations.

A simultaneous solution can be performed by writing a heat conduction equation applicable to both regions. This equation takes the form

$$C_p\rho \frac{\partial T}{\partial t} = \frac{\partial\left(K \frac{\partial T}{\partial Z}\right)}{\partial z} + \frac{1}{r} \frac{\partial\left(Kr \frac{\partial T}{\partial r}\right)}{\partial r}. \quad (7)$$

Expanding gives

$$\frac{\partial T}{\partial t} = \frac{K}{C_p\rho} \frac{\partial^2 T}{\partial Z^2} + \frac{K}{C_p\rho r} \frac{\partial T}{\partial r} + \frac{K}{C_p\rho} \frac{\partial^2 T}{\partial r^2} + \frac{1}{C_p\rho}\left(\frac{\partial K}{\partial Z} \frac{\partial T}{\partial Z} + \frac{\partial K}{\partial r} \frac{\partial T}{\partial r}\right). \quad (8)$$

The expanded equation is the same as Eq (1) except for the last two additional terms, which account for possible thermal conductivity gradients in the axial and radial directions. These gradients go to zero within either region and only have nonzero values on the regional boundaries.

Description of Thermal Model, Continued

Method of Solution for Regions 1 and 3 (cont'd)

Finite Difference Approximation

The fully implicit finite difference approximation to Eq (7) can be written using backward differences for calculational stability as

$$T_{I,J}^{N+1} - \frac{C_p\rho T_{I,J}^{N}}{\beta} + \frac{\Delta t K_{I,J}}{\beta \Delta Z^2}\left(T_{I,J+1}^{N+1} + T_{I,J-1}^{N+1}\right) \qquad (9)$$

$$+ \frac{\Delta t K_{I,J}}{\beta \Delta r^2}\left(T_{I+1,J}^{N+1} + T_{I-1,J}^{N+1}\right)$$

$$- \frac{\Delta t K_{I,J}}{\beta r \Delta r} T_{I-1,J}^{N+1}$$

$$- \frac{\Delta t}{\beta \Delta Z^2}\left(K_{I,J} - K_{I,J-1}\right) T_{I,J-1}^{N+1}$$

$$- \frac{\Delta t}{\beta \Delta r^2}\left(K_{I,J} - K_{I-1,J}\right) T_{I-1,J}^{N+1}$$

where

$$\beta = C_p\rho + \frac{2\Delta t K_{I,J}}{\Delta Z^2} + \frac{2\Delta t K_{I,J}}{\Delta r^2} - \frac{\Delta t K_{I,J}}{r \Delta r}$$

$$- \frac{\Delta t}{\Delta Z^2}\left(K_{I,J} - K_{I,J-1}\right) - \frac{\Delta t}{\Delta r^2}\left(K_{I,J} - K_{I-1,J}\right).$$

Note on Thermal Properties

Thermal properties are assumed to be independent of time (temperature and pressure invariant). We plan to investigate the effects of temperature-dependent material properties in a future study.

Boundary Conditions

The boundary conditions needed to solve Eq (7) are the same as those described for solving Region 1 (salt model).

Modeling the Cavern Fluids

Fluid Solution Method

Modeling the fluid region is much more complex than modeling the salt or the porous media annulus. Complications are produced by the following factors:

- Irregular wall geometry and the height of the cavern
- Forced convection during oil-fill of the caverns
- Free convection driven by the geothermal gradient
- Heat transfer across the oil/brine interface
- Heat transfer from an insoluble rubble bed underlying the saturated brine
- Heat transfer between the oil and brine during fill or withdrawal

Description of Thermal Model, Continued

Modeling the Cavern Fluids (cont'd)

Effects of Wall Geometry

In some cases, e.g., Sulphur Mines Cavern 7 (SM-7) (Figure 5), the wall geometries of the SPR caverns are irregular. Exact modeling of such complex geometries requires a full three-dimensional capability. Rather than using a three-dimensional method, we are accounting for variations in cavern radii by using a slanted boundary condition for the heat flux entering an adjacent fluid cell (using the heat flux component normal to the boundary). This method should have little influence on the calculations for Phase 1, 2, and 3 caverns which are reasonably cylindrical. The effect of very irregular cavern shapes will be assessed in the future, using comparisons between experimental data and thermal model calculations. A second problem associated with the cavern wall results from the overall cavern size. To accommodate ten million barrels (10 MMBBL) of oil, the height of most of the caverns exceeds 2000 ft (from total depth to the top of the cavern). In the presence of a normal geothermal gradient (linearly increasing temperature with depth), oil near the bottom of the cavern is hotter and thus less dense than oil at a higher elevation. Buoyancy forces cause the lighter oil to rise along the cavern wall (free convection). For relatively small travel distances this type of behavior is fairly well treated, using either laminar or turbulent boundary layer equations. However, with a scaling depth (L) of 1000 ft, the Rayleigh number for a vertical surface,[7] $\left(\mathrm{Ra} = \frac{g\beta\Delta T L^3}{\nu\alpha}\right)$ is $\sim 10^{16}$. The Rayleigh number is the product of the Grashof number $\left(\mathrm{Gr} = \frac{g\beta\Delta T L^3}{\nu^2}\right)$ times the Prandtl number $\left(\mathrm{Pr} = \frac{C_p\mu}{K}\right)$ and gives an indication of the relative magnitude of the buoyancy and viscous forces in the fluid. Flows having a Ra = 10^{16} are highly turbulent (point of turbulent/laminar transition = 10^9) and are extremely difficult to model because of instabilities in the numerical solution methods.

Because of this difficulty, we modeled the fluid region using the one-dimensional Rahm-Walin technique[8-10] employed in the Sandia salt-leach model, SANSMIC.[11] The Rahm-Walin method is an approximate theory for treating combined convection in stable, stratified enclosures where the natural convection is induced by wall sources weak enough so that the variations in the thermal or concentration boundary layer are smaller than the total variation caused by the stratification. All effects of density variations are accounted for in the buoyancy term (Boussinesq approximation).[9] The one-dimensional, time-dependent Rahm-Walin equation for temperature can be written as

$$\frac{\partial T}{\partial t} = \frac{\alpha\partial^2 T}{\partial Z^2} - \left(\frac{M_o}{A} - \frac{\alpha\partial A}{A\partial Z}\right)\frac{\partial T}{\partial Z} - \frac{\alpha}{A}\oint \frac{S_o\,(T - \hat{T})}{r\cos\theta}\,dl\,. \tag{10}$$

Expanding the terms and evaluating the line integral (axial symmetry and constant material properties) in Eq (10) gives

$$\frac{\partial T}{\partial t} = \frac{\alpha\partial^2 T}{\partial Z^2} - \left(\frac{M_o}{A} - \frac{2\alpha}{r}\frac{\partial r}{\partial Z}\right)\frac{\partial T}{\partial Z} - \frac{2\alpha S_o}{r\cos\theta}\,(T - \hat{T})\,. \tag{11}$$

Modeling the Cavern Fluids (cont'd)

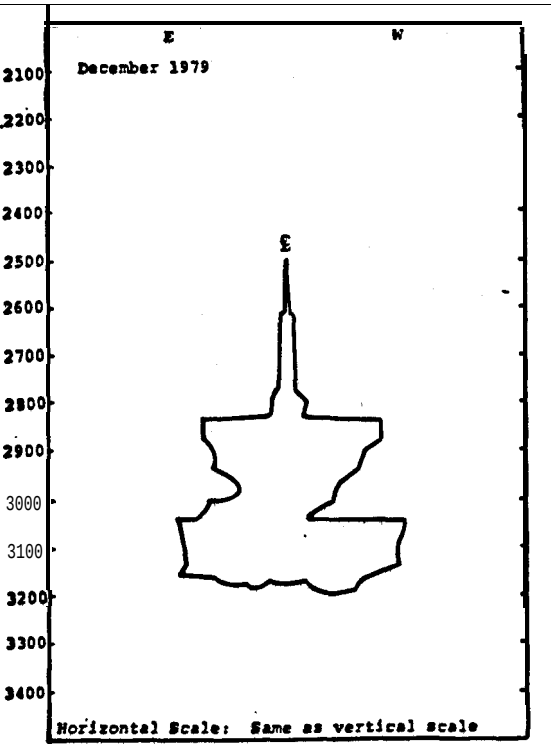

Figure 5. Sulphur Mines Cavern 7

The terms on the right-hand side of Eq (11) have the following significance: term 1 represents axial heat conduction; term 2 represents heat transfer due to forced convection and radial geometry changes; and term 3 represents heat transfer from the wall to a limited thickness boundary layer,

Modifications to the Rahm-Walin Equation

Two modifications were made to the Rahm-Walin equation to improve the predictive capability of the model:

- A modification to incorporate two immiscible fluids: oil and saturated brine
- A modification to simulate enhanced heat transfer across the oil/brine interface

These modifications will be discussed below.

Multimaterial Modification

To account for the difference between oil and saturated brine, the Rahm-Walin equation was modified to

$$\frac{\partial T}{\partial t} = \frac{1}{C_p \rho} \frac{\partial \left(K \frac{\partial T}{\partial Z} \right)}{\partial Z} - \left(\frac{M_o}{A} - \frac{2\alpha \partial r}{r \partial Z} \right) \frac{\partial T}{\partial Z} - \frac{2\alpha S_o}{r \cos \theta} (T - \hat{T}) . \qquad (12)$$

This modification introduces a thermal conductivity gradient in the axial direction that is nonzero only on the interface between the oil and brine.

Modeling the Cavern Fluids (cont'd)

Interfacial Heat Transfer

In the absence of enhanced interfacial heat transfer, our thermal model predicts a fairly large temperature drop across the interface that is not observable in any of the experimental data. To correct this problem, we added a heat transfer term that augments the energy transferred across the oil/brine interface. We believe that this enhanced heat transfer is produced by the action of countercurrent-flowing fluids at the interface. (Oil is moving from the cavern center to the cavern wall, while the brine is moving from the wall to the cavern center. We assume these motions are a part of large, free-convection cells established by buoyancy effects in the cavern.)

The modified Rahm-Walin equation, including the added interfacial heat transfer term, is written as

$$\frac{\partial T}{\text{at}} = \frac{1}{C_p \rho} \frac{\partial\left(K \frac{\partial T}{\partial Z}\right)}{\partial Z} - \left(\frac{M_o}{A} - \frac{2\alpha \partial r}{r \partial Z}\right)\frac{\partial T}{\partial Z} - \frac{2\alpha S_o}{r \cos\theta}(T - \hat{T}) + S \quad (13)$$

where S is a source term applied only at the oil/brine interface.

Source Term Model

The temperature change, with respect to time caused by a source term, can be simply expressed as

$$\frac{\partial T}{\text{at}} = \frac{HA\Delta T}{\rho C_p V} = S \quad (14)$$

where H = heat transfer coefficient and V is the volume of the region.

Empirically, H = K Nu/L where Nu = the average Nusslet number.

$$S = \frac{KNuA\Delta T}{L\rho C_p V} = \frac{\alpha NuA\Delta T}{LV} \quad (15)$$

As an approximation, we treat the direct-contact heat exchange process at the interface as if the oil were freely convecting across a hot, flat semicircular surface. The Nusselt number for such a flow is given by the following expression:[5]

$$Nu = \frac{hL}{K} \simeq 0.27\ Ra" \quad (16)$$

and the Rayleigh number, Ra, is given by the usual expression:

$$Ra = \frac{g\beta\,(T_s - T_\infty)L^3}{\nu\alpha} \quad (17)$$

Modeling the Cavern Fluids (cont'd)

For a cylindrical cavern a cross-sectional cut perpendicular to the major axis is circular and L, the characteristic length (A/P,) = r/2, where **r** is the cavern radius. The resulting source term is thus expressed as

$$S = \frac{\alpha\, NuA\Delta T}{LV} = \frac{2\,\alpha\, Nu\Delta T}{RAZ}. \tag{18}$$

Finite Difference Form for Eq (13)

Eq (13) can be approximated by the following fully implicit, finite difference expression:

$$\left(\frac{T_J^{N+1} - T_J^N}{\alpha\Delta t}\right) = \frac{T_{J+1}^{N+1} + T_{J-1}^{N+1}}{\Delta Z^2} - \frac{2\,T_J^{N+1}}{\Delta Z^2} \tag{19}$$

$$- \left(\frac{M_o}{\alpha A} - \frac{2}{r}\frac{(r_{I+1} - r_{I-1})}{2AZ} + C\right)\frac{(T_J^{N+1} - T_{J-1}^{N+1})}{AZ}$$

$$- \frac{2}{r\cos\theta}\frac{K_{salt}}{K_{oil/brine}\,Ar\cos\theta}(T_J^{N+1} - \hat{T}_J^N)$$

$$+ \frac{2Nu}{r\Delta Z}(T_J^N - T_{J-1}^N)$$

where

$$C = \frac{1}{C_p\rho}\left(\frac{K_{J+1} - K_J}{\Delta Z}\right).$$

Comments

The following comments apply to Eq (19):

- A backward difference scheme is used to approximate the thermal gradient $\frac{\partial T}{\partial Z}$ to promote calculation stability.[12]
- A fully implicit method was employed to match the method used in the salt annulus and porous media region, and to allow the large time steps necessary for making long-term temperature predictions.
- The last term of the equation is applied only at the oil/brine interface.

Boundary Conditions

The following boundary conditions are required to solve Eq (19):

- Initial temperature of the fluid
- Temperature or heat flux at the cavern wall
- Temperatures or heat fluxes at the top and bottom of the cavern.

Modeling the Cavern Fluids (cont'd)

Initial Fluid Temperature

The initial temperature of the cavern fluid is not generally well known. In our letter to E. E. Chapple,' we recommended measuring the temperature of the oil at the time of cavern fill, before and after any large volumetric changes, and at regular six-month intervals.

For our calculations, we assumed that oil enters a cavern at a temperature of 70°F. A heat exchanger model is used to account for heat transfer to the oil during fill from counter current-flowing brine, which is at a higher temperature.

We are presently determining the effects of variations in the initial fluid temperatures. These results will be reported as part of a general thermal model sensitivity study.

Flux at the Cavern Wall

At a cavern wall, the following Rahm-Walin approximation is made:

$$\left.\frac{\partial T}{\partial \ell}\right|_{\ell = 0} = S_o\,(T - \hat{T}) \tag{20}$$

where S_o is defined as $\frac{K_{salt}}{K_{oil/brine}\, r \cos(\theta)}$ and ℓ measures the distance from the wall along the inward normal to the boundary. The cos (θ) term accounts for the possibility of irregularly shaped walls and $\hat{T}$ is the salt temperature at the boundary. Heat transfer from the salt massif to the fluids is conduction limited.

Boundary Conditions at the Top and Bottom of the Cavern

Temperatures at the top and the bottom of the cavern are obtained by using a fully implicit expression:

$$\frac{\partial T}{\partial t} = \frac{1}{C_p \rho} \frac{\partial \left(K \frac{\partial T}{\partial Z} \right)}{\partial Z}. \tag{21}$$

In finite difference format, this equation becomes

$$\frac{(T_B^{N+1} - T_B^N)}{At} = \frac{K}{C_p \rho} (T_{B+1}^{N+1} + T_{B-1}^{N+1} - 2T_B^{N+1}) \tag{22}$$

$$+ \frac{1}{C_p \rho} \frac{(K_{B+1} - K_B)}{AZ} \frac{(T_{B+1}^{N+1} - T_B^{N+1})}{AZ}$$

where subscript B indicates boundary.

Use of a conduction-limited boundary condition is not completely correct (there may be some convective heat transfer due to fluid flow). However, we found that the Rahm-Walin calculations in the fluid were insensitive to the bottom and top boundary temperatures.

Description of Thermal Model, Continued

Modeling the Cavern Fluids (cont'd)

Fluid Properties

Fluid thermal properties were treated as constants. Brine properties were assumed to be those of a saturated solution at 100°F, and the oil properties were assumed to be equivalent to a standard oil model at 100°F. Table 2 lists all relevant fluid and salt properties used in the model. Our sensitivity study will investigate the variation effects of material property with temperature and pressure.

Rayleigh-Taylor Model for Fluid Region

The results of the Rahm-Walin calculations model can produce an unstable stratified condition in which cooler fluid overlies hotter, less dense fluid. In our model, we allow the hotter fluid to rise and mix with the cooler material. Mixing is performed under the constraint of constant energy. If the cavern narrows as it rises, we have also incorporated a fluid roll-over model to ensure proper mixing. The fluid roll-over model has an upper cell and a lower cell. The upper cell has a smaller volume than the lower cell and, initially, the lower cell is filled with warmer fluid. During one time step, the entire fluid volume of the upper cell is replaced with fluid from the lower cell. Excess warm fluid (equal to the difference in cell volumes) remains in the lower cell. The cooler fluid from the upper cell enters the lower cell and equilibrates with the excess, warmer fluid.

Energy Balance Model

To conserve energy, the total energy of the mixed system is compared to the energy the system would have, because of forced convection and heat transfer across the boundary. If the energies are not equal, the energy of the system is corrected by a multiplier equal to the ratio of the system energy to the energy input to the system over one time step. Typically, this multiplier is within 0.001 of 1.0.

Heat Exchanger Model

Overview

During the fill or drawdown operations, oil and brine flow in and out of the cavern through concentric pipes in opposite directions with the brine flowing through the inner tube and the oil through the outer. During fill, cool oil flows into the cavern while saturated brine at a higher temperature flows out. During drawdown this process is reversed. Thus, the cavern fluids form a counterflow heat exchanger that effectively operates from ground level to the top of the cavern (overall length ~ 2000 ft). Since a significant amount of heat can be exchanged in this process, we incorporated a log-mean temperature difference heat exchanger model to simulate oil or brine heat-up during fill or drawdown.

Heat Exchanger Model

For a counterflow heat exchanger, the amount of heat transferred from one fluid to another, Q, can be determined from the following equations?

$$Q = \dot{m}_h C_{ph} (T_{hi} - T_{ho}) \quad (23)$$

$$Q = \dot{m}_c C_{pc} (T_{co} - T_{ci}) \quad (24)$$

$$Q = UAAT, \quad (25)$$

Heat Exchanger Model, Continued

Heat Exchanger Model (cont'd)

where

A = heat exchanger area
$\dot{m}_h$ = hot fluid mass flux
$\dot{m}_c$ = cold fluid mass flux
C_{ph} = specific heat capacity of the hot fluid
C_{pc} = specific heat capacity of the cold fluid
T_{hi} = inlet temperature of the hot fluid
T_{ho} = outlet temperature of the hot fluid
T_{ci} = inlet temperature of the cold fluid
T_{co} = outlet temperature of the cold fluid
U = overall heat transfer coefficient
AT_m = log-mean temperature difference.

Log-Mean Temperature Difference

In a counterflow heat exchanger, the log-mean temperature difference, AT,, is defined by the following expression:

$$AT, = \frac{AT, - AT,}{\ell n\,(\Delta T_2/\Delta T_1)} \qquad (26)$$

where

$$\Delta T_2 = T_{ho} - T_{ci}$$

$$\Delta T_1 = T_{hi} - T_{co}\ .$$

Overall Heat Transfer Coefficient

If we neglect the effect of the wall separating the two fluids and assume adiabatic conditions (zero heat flow) for the outermost pipe wall casing, the overall heat transfer coefficient for the heat exchanger is

$$U = \frac{1}{\frac{1}{h_o} + \frac{r_o}{r_i\, h_i}} \qquad (27)$$

where

r_o = outer radius of the outer tube
r_i = inner radius of the inner tube
h_o = heat transfer coefficient for the outer tube
h_i = heat transfer coefficient for the inner tube.

Heat Exchanger Model, Continued

Local Heat Transfer Correlations

For smooth pipes and turbulent flow, the local heat transfer coefficient, H, can be obtained from the Dittus-Boelter correlation as[13]

$$H = 0.023\ R_e^{0.8}\ P_r^N\ K/D \qquad (28)$$

where

N = 0.4 for heating or N = 0.3 for cooling
D = hydraulic diameter of the pipe
K = thermal conductivity
R_e = fluid Reynolds number
P_r = fluid Prandtl number = $\frac{C_p \mu}{K}$.

Average Heat Transfer Correlations

For L/D>60, the above correlations can be used to represent the average heat transfer coefficient for the entire length of the heat exchanger. Since the outer diameter of the pipe is less than 1 ft and the overall length is ~2000 ft, the above condition is easily satisfied.

Hydraulic Diameters

The hydraulic diameter is defined by the expression

$$D = 4\ A/P_w \qquad (29)$$

where

A = flow area
P_w = wetted perimeter.

The hydraulic diameters for the inner and outer pipes are thus 2 r_i and 2 $(r_o - r_i)$, respectively.

Method of Solution

Since we know only the inlet temperatures to the heat exchanger, we used an iterative solution to find the transcendental outlet temperatures. Because of the rapid convergence of the numerical algorithm (typically requiring < 10 iterations to meet the 0.00001 convergence criteria) and because the heat exchanger model is called only once per calculation, a more elaborate method such as the number of transfer units (NTU) was not used.[5]

Temperature-Dependent Properties

Sample calculations performed for cavern conditions indicate that during fill, the temperature of the oil entering the cavern can be more than 25°F warmer than the oil at ground level. The actual increase in temperature is a function of flow rate, material properties, and geometry. The observed temperature increase can significantly affect the oil viscosity and Prandtl number, $\frac{C_p \mu}{K}$.

During drawdown, the entering brine experiences a similar heat-up, but to a lesser extent. Other fluid properties (density, thermal conductivity, and specific heat capacity) are not significantly affected by the temperature increase and are assumed to be constant.

Heat Exchanger Model, Continued

Incorporating Temperature-Dependent Properties

To account for the temperature dependence in the fluid viscosity and Prandtl number, a reference temperature was used.

Reference Temperature Method

In the reference temperature method, the initial temperatures of both the saturated brine and the oil are assumed to be equal to the mean inlet temperature:

$$\bar{T} = \frac{(T_{ci} + T_{hi})}{2}. \tag{30}$$

Outlet temperatures are then calculated, assuming fluid properties at the mean inlet temperature. An iteration is then performed using the newly calculated outlet temperatures in the averaging process:

$$\bar{T}_{oil} = \frac{(T_{oil\ in} + T_{oil\ out})}{2} \tag{31}$$

and

$$\bar{T}_{brine} = \frac{(T_{brine\ in} + T_{brine\ out})}{2} \tag{32}$$

Reference Temperature Method (cont'd)

These new average temperatures are then used to calculate the next set of outlet temperatures. This process is continued until the average temperatures are within some specified convergence criteria.

Convergence

The average pipe temperatures converged to within $0.01°F$ after two iterations. This convergence is sufficiently accurate for the assumptions of the heat exchanger model.

Thermal Model Comparisons

Overview

In this section we compare our thermal model predictions with experimental data from the following SPR caverns:

. WH-11
- BM-4

The following comparisons will be made:

- A full-axial temperature profile comparison at a given time (usually the most current thermal log)
- A comparison of temperatures at three specified locations in the cavern for all thermal measurements.

In addition, we will show the predicted axial temperature profile behavior as a function of time for both caverns.

Comparisons With Experimental Data From WH-11

Background

WH-11 was chosen as the first SPR cavern for thermal model assessment because of the following features that make it unique:

- The geometry of the cavern is nearly cylindrical (Figure 6).
- It has been oil-filled for over three years.
- It has a well-documented thermal history.

WH-11 Parameters

Table 4 summarizes the relevant physical parameters of WH-11. Material properties correspond to those listed in Table 2.

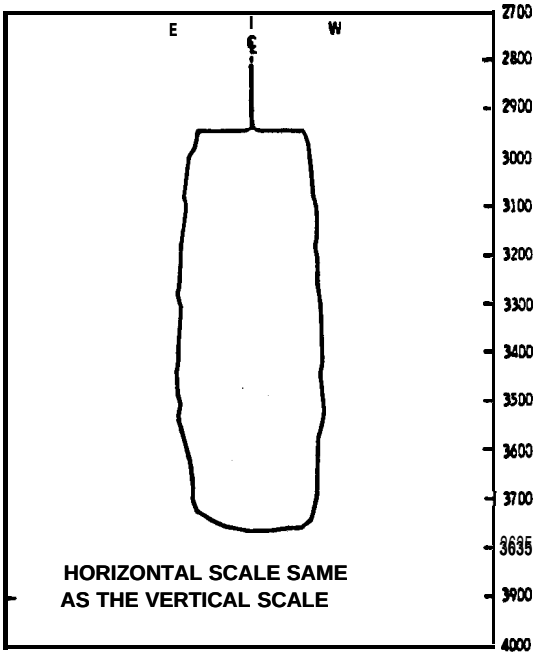

Figure 6. West Hackberry Cavern 11

Comparisons With Experimental Data From WH-11 (cont'd)

Table 4. Physical Properties of WH-11

Volume: 8.5 MMBBL
Top of cavern: 2945 ft
Bottom of cavern: 3760 ft
Top of salt: 2056 ft
Approximate date of fill: November 1980
Geothermal gradient: 1.67°F/100 ft
Oil temperature at fill: 70°F
initial brine temperature: 70°F
Temperature at bottom of calculation region (3940 ft): 141°F

Height (ft)	Radius (ft)
0.0	111.750 (Depth = 3760 ft)
20.0	124.020
40.0	127.910
60.0	128.940
80.0	129.540
100.0	131.020
120.0	132.620
140.0	134.360
160.0	138.300
180.0	142.850
200.0	146.200
220.0	147.780
240.0	147.920
260.0	147.790
280.0	147.800
300.0	147.850
320.0	147.720
340.0	147.540
360.0	147.140
380.0	146.930
400.0	146.480
420.0	145.590
440.0	144.810
460.0	143.920
480.0	142.980
500.0	142.710
520.0	142.310
540.0	140.910
560.0	139.760
580.0	138.810
600.0	137.610
620.0	136.620
640.0	135.540
660.0	134.190
680.0	132.530
700.0	130.300
720.0	127.610
740.0	122.910
760.0	117.060
780.0	112.510
800.0	3.970
820.0	0.920

Comparisons With Experimental Data From WH-11 (cont'd)

Fill History

In addition to the cavern's physical parameters and material properties, a fill history is required in order to model forced convection heat transfer. Figure 7 shows an approximation of the fill history for WH-11. We modeled the WH-11 fill history shown in Figure 7 with the sequence in Table 5.

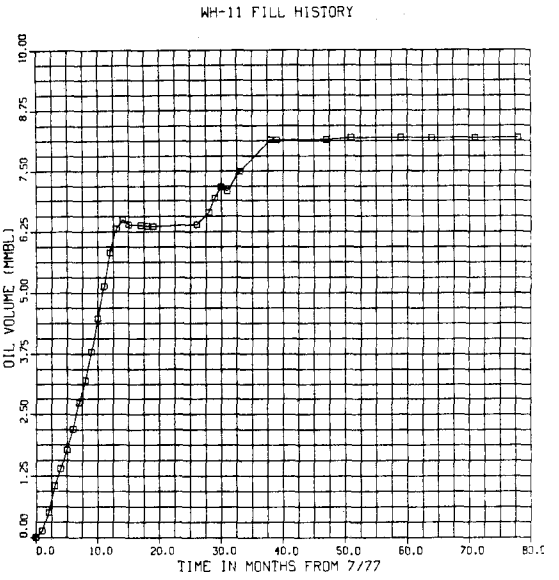

Figure 7. Fill History of WH-11

Table 5. Fill History Model for WH-11

Step	Time	Comments
1	O-24 months	All brine (Time 0 = mid-1975)
2	24-38 months	Reverse oil fill (15,024 bbl/day)
3	38-61 months	No fill (constant oil level)
4	61-73 months	Reverse oil fill (4980 bbl/day)
5	73-102 months	No fill to present (Jan. 1984)

Porosity of Anhydrite Layer

We assumed that the porosity (ϕ) of the anhydrite/brine layer underlying the cavern is 30%. This value was chosen for the following reasons:

- It is typical of the value expected.
- Variations in this value did not significantly affect the calculation.

Comparisons With Experimental Data From WH-11 (cont'd)

Comparison of Model Results With Experimental Data

Figure 8 compares our model temperatures with a thermal log performed in January 1984. The extensive isothermal region beginning at -3000 ft and extending downward to the oil/brine interface is well predicted by the model, with the isothermal model temperature being within 2% of the measured value.

This result is very good considering the uncertainties in the model created by the initial oil temperature, and uncertainties in the geothermal gradient, in the physical parameters of the system, and in the experimental measurements. These uncertainties are discussed in detail in our letter to E. E. Chapple.'

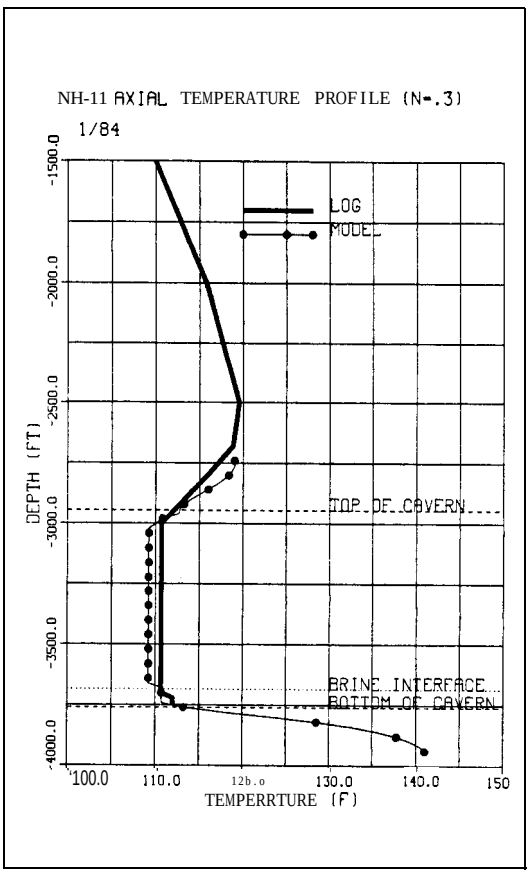

Figure 8. Comparison of WH-11 Model Temperatures With a Thermal Log Performed in January 1984

Time-Dependent Comparisons

Figures 9, 10, and 11 show comparisons made between the thermal model and four thermal logs at three different elevations: 20,360, and 620 ft from the bottom of the cavern. Sharp discontinuities in the model temperature profile correspond to the oil filling schedule. Although the number of thermal logs is limited, the thermal model is correctly predicting the trends observed in the experimental data. Note the slower heat-up in the oil compared to the brine. This is caused by differences in the material's thermal properties (the oil-full cavern heats up more slowly than the brine-full cavern).

Thermal Model Comparisons, Continued

Comparisons With Experimental Data From WH-11 (cont'd)

Axial Profiles as a Function of Time

Figure 12 compares the axial temperature profiles produced by our model at 27, 39, and 102 months. These times correspond to the beginning of the initial oil fill, the end of the initial oil fill, and conditions in January 1984. As expected, the temperature near the middle of the cavern rises slowly with time, and the oil/brine interface moves downward with increasing oil volume.

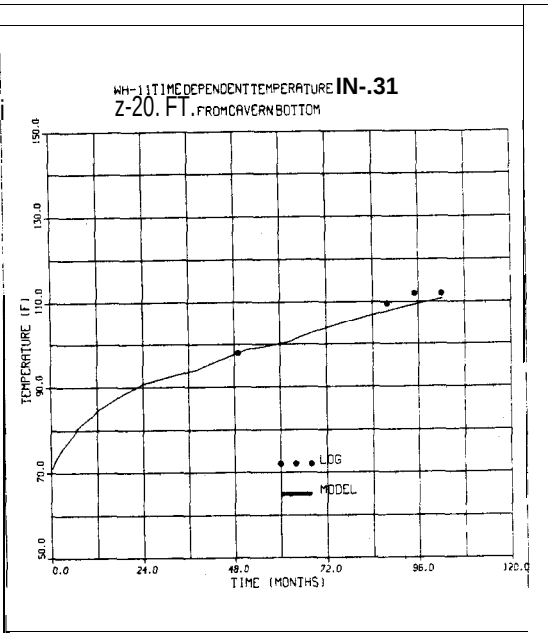

Figure 9. Comparison of WH-11 Model With Four Thermal Logs at a 20-ft Elevation

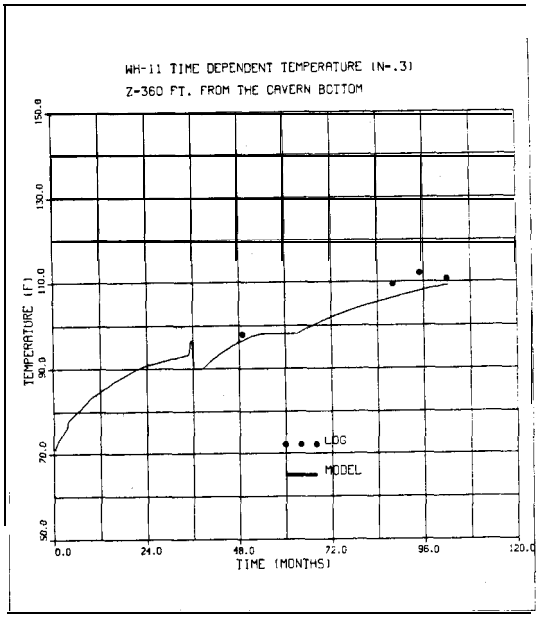

Figure 10. Comparison of WH-11 Model With Four Thermal Logs at a 360-ft Elevation

Thermal Model Comparisons, Continued

Comparisons With Experimental Data From WH-11 (cont'd)

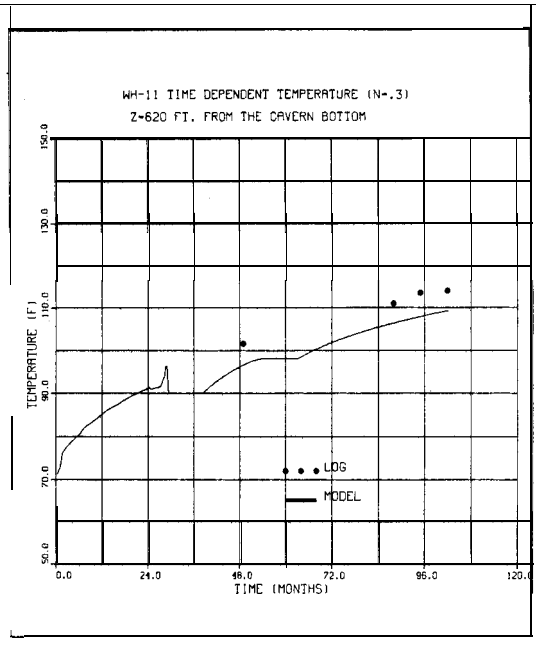

Figure 11. Comparison of WH-11 Model With Four Thermal Logs at a 620-ft Elevation

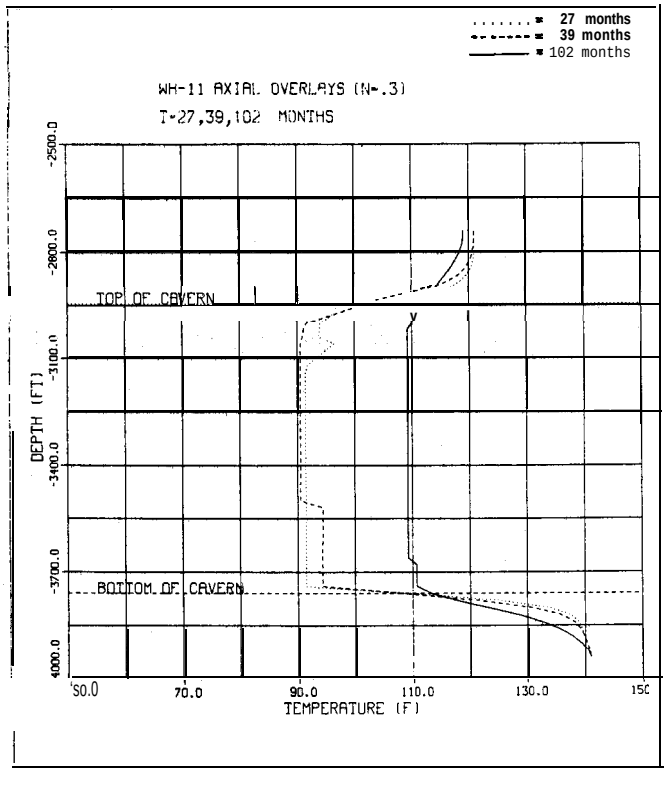

Figure 12. Axial Temperature Profiles of WH-11 Model at 27, 39, and 102 Months

Thermal Model Comparisons, Continued

Comparisons With Experimental Data From BM-4

Background

BM-4 (Figure 13) was chosen as the second SPR cavern for thermal model assessment for the following reasons:

- Its shape allows us to examine the effect of slanted boundary conditions.
- It has been thermally logged three times since the beginning of fill.
- It is volumetrically large.

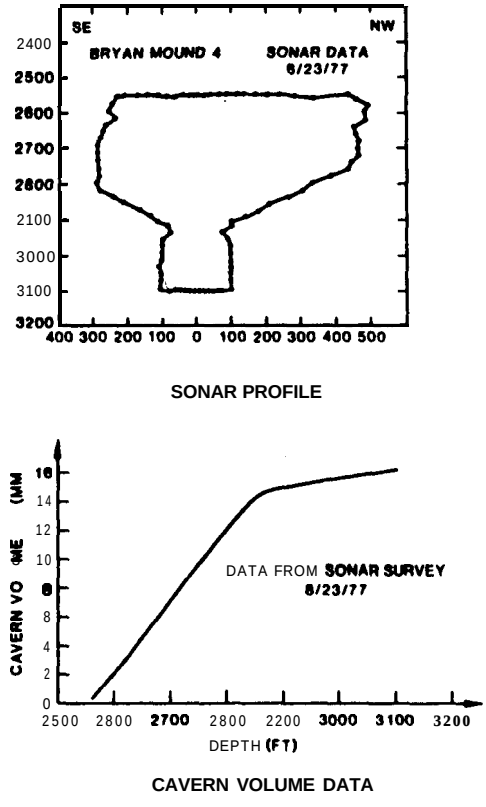

Figure 13. Bryan Mound Cavern 4

Comparisons With Experimental Data From BM-4 (cont'd)

BM-4 Parameters

Table 6 summarizes the relevant physical parameters for BM-4. Its material properties are listed in Table 2.

Table 6. Physical Properties of BM-4

Volume: 17.5 MMBBL
Top of cavern: 2555 ft
Bottom of cavern: 3107 ft
Top of salt: 1067 ft
Approximate date of fill: August 1981
Geothermal gradient: 1.4°F/100 ft
Oil temperature at fill: 70.0°F
Initial brine temperature: 75.0°F
Temperature at the bottom of the calculational region: 145°F

Height (ft)	Radius (ft)
0.0	102.0
28.0	101.2
56.0	101.5
84.0	100.7
112.0	98.1
140.0	84.8
168.0	94.6
196.0	152.3
224.0	204.9
252.0	271.4
280.0	297.8
308.0	312.8
336.0	325.4
364.0	327.5
392.0	326.8
420.0	318.2
448.0	310.7
476.0	314.9
504.0	312.2
532.0	312.1
550.0	308.6

Thermal Model Comparisons, Continued

Comparisons With Experimental Data From BM-4 (cont'd)

Fill History

Figure 14 shows the fill history for BM-4. We modeled this fill history following the sequence given in Table 7.

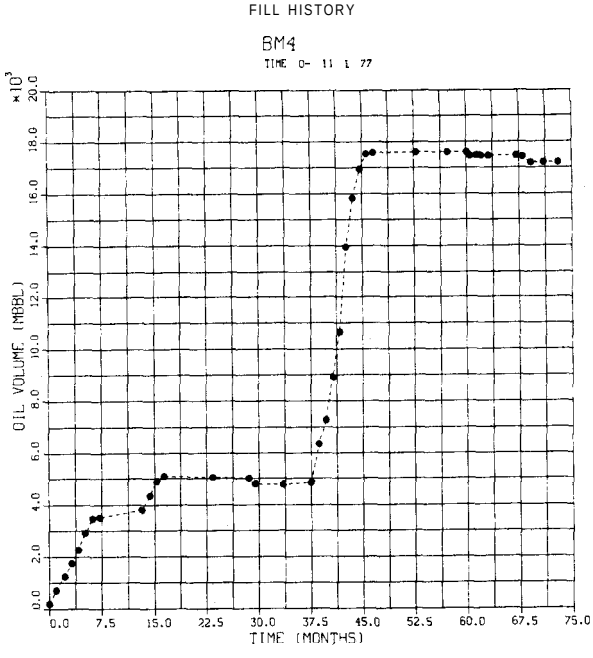

Figure 14. Fill History of BM-4

Table 7 Fill History Model for BM-4

Step	Time	Comments
1	O-33.3 months	All brine (Time 0 = Feb. 1975)
2	33.3-41.5 months	Fill at 20,160 bbl/day
3	41.5-72.1 months	No fill
4	72.1-80.3 months	Fill at 50,400 bbl/day
5	80.3 months-present	No additional fiil to present (Jan. 1984)

Porosity of Anhydrite Layer

A porosity of 30% was again used in this calculation.

Comparisons With Experimental Data From BM-4 (cont'd)

Comparisons of Model Results With Experimenal Data

Figure 15 shows a comparison of our model results with a thermal log performed in October 1982. Again, the agreement between the experimental data and the model predictions is very good. Large differences in temperature above the top of the cavern are expected because the measurement does not necessarily represent salt conditions.

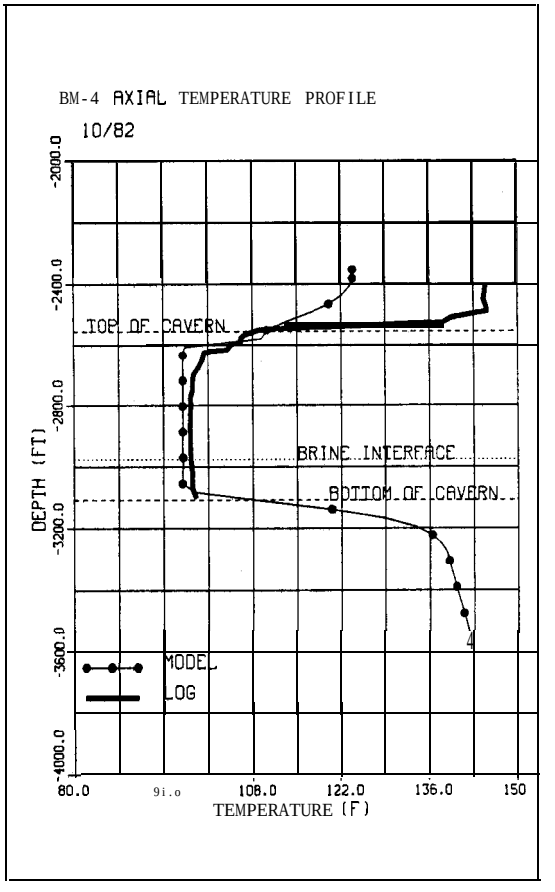

Figure 15. Comparison of BM-4 Model With a Thermal Log Performed in October 1982

Thermal Model Comparisons, Continued

Comparisons With Experimental Data From BM-4 (cont'd)

Time-Dependent Comparisons

Figures 16, 17, and 18 compare the BM-4 thermal model with three logs at locations of 20,280, and 500 ft from the bottom of the cavern. Except for the first log, the model adequately predicts the observed trends in the data.

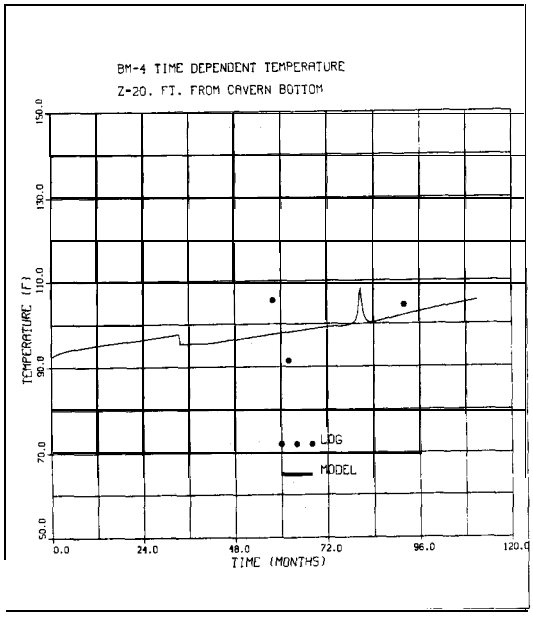

Figure 16. Comparison of BM-4 Model With Three Logs at a 20-ft Elevation

Comparisons With Experimental Data From BM-4 (cont'd)

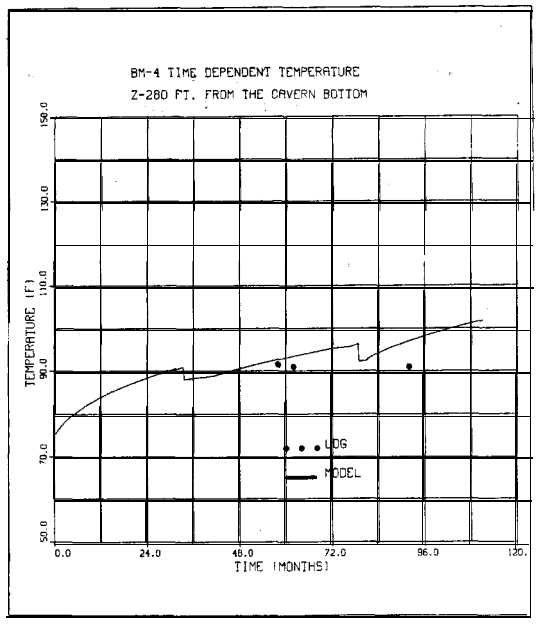

Figure 17. Comparison of BM-4 Model With Three Logs at a 280-ft Elevation

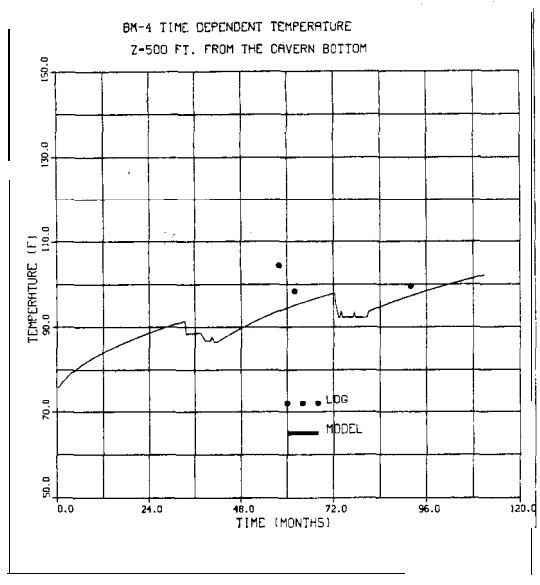

Figure 18. Comparison of BM-4 Model With Three Logs at a 500-ft Elevation

Comparisons With Experimental Data From BM-4 (cont'd)

Axial Profiles as a Function of Time

Figure 19 compares the axial temperature profiles produced by our model at 58, 92, and 106 months. A gradual increase in overall cavern temperature is evident.

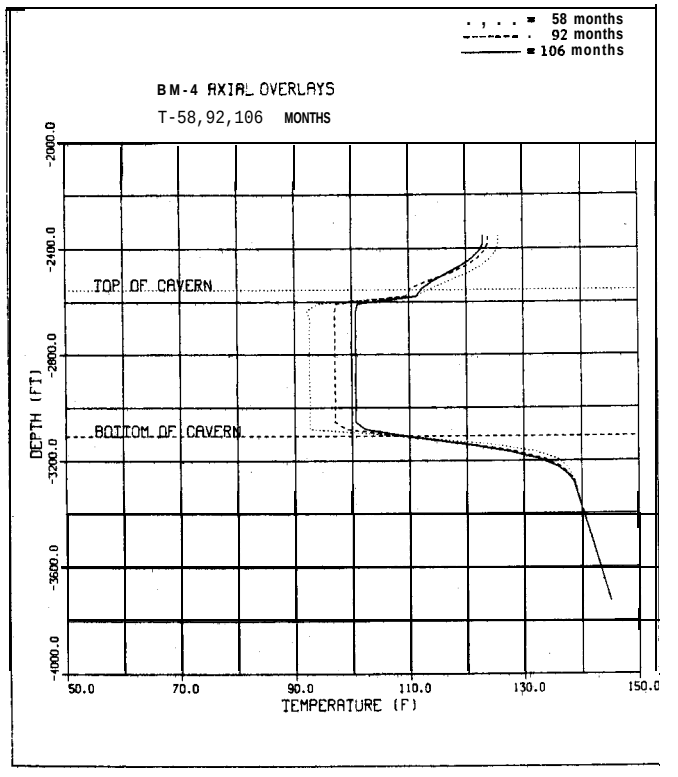

Figure 19. Vertical Temperature Profiles of BM-4 Model at 58, 92, and 106 Months

Summary of the Thermal Model

Summary

The Sandia thermal model combines a two-dimensional finite difference solution in the salt and porous media with a one-dimensional Rahm-Walin technique for the cavern fluids. The model employs constant mesh spacing and constant material properties. Comparisons between the model calculations and experimental data from WH-11 and BM-4 show fairly good agreement.

Possible Model Improvements

Possible improvements to our thermal model include

- Variable mesh spacing
- Temperature-dependent material properties
- Modeling the cavern fluid region with a two-dimensional model
- A thin cavern roof
- Cavern interactions

Current Efforts

In addition to investigating the above model improvements, we are performing a sensitivity study in order to map the response surface of the model. This study will allow us to determine the effect of individual parameter uncertainties on model calculations and to identify areas where improved measurements or physical models are required.

References

'J. K. Linn to E. E. Chapple, "SPR Thermal Data Assessments and Recommendations" (Albuquerque, NM: Sandia National Laboratories, 4 January 1984). Memorandum.

[2]R. M. Pytkowicz, ***Equilibra, Non-Equilibra, and Natural Waters,*** Vols I, II (New York: John Wiley and Sons, 1983).

[3]R A. Freeze and J. A. Cherry, ***Groundwater*** (Englewood Cliffs, NJ: Prentice-Hall, Inc., 1979).

[4]D. W. Kaufmann, "Sodium Cloride," ***ACS Monograph 145,*** American Chemical Society (Washington, DC: Reinhold Publishing Corp., 1960).

[5]F. P. Incropera and D. P. Dewitt, ***Fundamentals of Heat Transfer (New*** York: John Wiley and Sons, 1981).

[6]R. P. Tye, ***Thermal Conductivity*** (New York: Academic Press, 1969).

[7]E. R. G. Eckert and R. M. Drake, ***Analysis*** *of* ***Heat and Mass Transfer (New*** York: McGraw-Hill Book Co., 1972).

[8]G. Walin, "Contained Non-Homogeneous Flow Under Gravity or How to Stratify a Fluid in the Laboratory," ***J Fluid Mech,*** Pt. 4, 48:647-72 (1971).

[9]L Rahm and G. Walin, "Theory and Experiments on the Control of Stratification in Almost Enclosed Regions, ***J Fluid Mech,*** Pt. 2, 90:315-25 (1979).

[10]L. Rahm and G. Walin, "On Thermal Convection in Stratified Fluids," ***Geophys Astrophys Fluid Dynamics,*** 1979, Vol. B, pp 51-65.

"A. J. Russo, ***A User's Manual*** *for* ***the Salt Solution Mining Code, SANSMIC,*** SAND83-1150 (Albuquerque, NM: Sandia National Laboratories, 1983).

[12]J. D. Lawson and J. L. Morris, "The Extrapolation of First Order Methods for Parabolic Partial Differential Equations I," ***SIAM J. Numer Anal*** 15(6):1212-24 (1978).

[13]J. G. Collier, *Convective* ***Boiling and Condensation*** (Maidenhead, Berkshire, England: McGraw-Hill Book Co. (UK) Limited, 1972).

DISTRIBUTION:

US Department of Energy (10)
Strategic Petroleum Reserve, PMO
Attn: E. E. Chapple. PR-632 (8)
TDCS, L. Smith (2)
900 Commerce Rd East
New Orleans, LA 70123

US Department of Energy (2)
Strategic Petroleum Reserve
Attn: D. Johnson
D. Smith
1000 Independence Ave SW
Washington, DC 20585

US Department of Energy
Oak Ridge Operations Office
Attn: P. Brewington, Jr.
PO Box E
Oak Ridge, TN 37831

Aerospace Corporation (2)
Attn: K. Henrie
R. Merkle
800 Commerce Rd East, Suite 300
New Orleans, LA 70123

Walk-Haydel & Associates
Attn: R. Haney
600 Carondelet
New Orleans, LA 70112

POSSI (2)
Attn: K. Mills
850 S. Clearview Pkwy
New Orleans, LA 70123

1512	J. C. Cummings
1521	R. D. Krieg
1542	B. M. Butcher
1821	N. E. Brown
6200	V. L. Dugan
6250	B. W. Marshall
6257	J. K. Linn (10)
6257	D. Tomasko (10)
8024	M. A. Pound
3141	C. M. Ostrander (5)
3151	W. L. Garner
3154-3	C. H. Dalin (28)
	For DOE/TIC (Unlimited Release)